



This is a repository copy of *Considerations using additive manufacture of emulsion inks to produce respiratory protective filters against viral respiratory tract infections such as the COVID-19 virus.*

White Rose Research Online URL for this paper:  
<http://eprints.whiterose.ac.uk/170336/>

Version: Published Version

---

**Article:**

Sherborne, C. and Claeysens, F. [orcid.org/0000-0002-1030-939X](https://orcid.org/0000-0002-1030-939X) (2021) Considerations using additive manufacture of emulsion inks to produce respiratory protective filters against viral respiratory tract infections such as the COVID-19 virus. *International Journal of Bioprinting*, 7 (1). 316. ISSN 2424-7723

10.18063/ijb.v7i1.316

---

**Reuse**

This article is distributed under the terms of the Creative Commons Attribution-NonCommercial (CC BY-NC) licence. This licence allows you to remix, tweak, and build upon this work non-commercially, and any new works must also acknowledge the authors and be non-commercial. You don't have to license any derivative works on the same terms. More information and the full terms of the licence here:  
<https://creativecommons.org/licenses/>

**Takedown**

If you consider content in White Rose Research Online to be in breach of UK law, please notify us by emailing [eprints@whiterose.ac.uk](mailto:eprints@whiterose.ac.uk) including the URL of the record and the reason for the withdrawal request.



[eprints@whiterose.ac.uk](mailto:eprints@whiterose.ac.uk)  
<https://eprints.whiterose.ac.uk/>

## RESEARCH ARTICLE

# Considerations Using Additive Manufacture of Emulsion Inks to Produce Respiratory Protective Filters Against Viral Respiratory Tract Infections Such as the COVID-19 Virus

Colin Sherborne, Frederik Claeyssens\*

The Kroto Research Institute, North Campus, University of Sheffield, Broad Lane, Sheffield, S3 7HQ, UK

**Abstract:** This review paper explores the potential of combining emulsion-based inks with additive manufacturing (AM) to produce filters for respiratory protective equipment (RPE) in the fight against viral and bacterial infections of the respiratory tract. The value of these filters has been highlighted by the current severe acute respiratory syndrome coronavirus-2 crisis where the importance of protective equipment for health care workers cannot be overstated. Three-dimensional (3D) printing of emulsions is an emerging technology built on a well-established field of emulsion templating to produce porous materials such as polymerized high internal phase emulsions (polyHIPEs). PolyHIPE-based porous polymers have tailorable porosity from the submicron to 100 s of  $\mu\text{m}$ . Advances in 3D printing technology enables the control of the bulk shape while a micron porosity is controlled independently by the emulsion-based ink. Herein, we present an overview of the current polyHIPE-based filter applications. Then, we discuss the current use of emulsion templating combined with stereolithography and extrusion-based AM technologies. The benefits and limitation of various AM techniques are discussed, as well as considerations for a scalable manufacture of a polyHIPE-based RPE.

**Keywords:** Polymerized high internal phase emulsions; Emulsion templating; COVID-19; Additive manufacturing; Respirator protective equipment

\*Correspondence to: Frederik Claeyssens, The Kroto Research Institute, North Campus, University of Sheffield, Broad Lane, Sheffield, S3 7HQ, UK; F.Claeyssens@sheffield.ac.uk

**Received:** October 20, 2020; **Accepted:** November 18, 2020; **Published Online:** xxx

**Citation:** Sherborne C, Claeyssens F, 2021, Considerations using additive manufacture of emulsion inks to produce respiratory protective filters against viral respiratory tract infections such as the COVID-19 virus. *Int J Bioprint*. DOI: 10.18063/ijb.v7i1.316

## 1. Introduction

Personal protective equipment (PPE) and respiratory protective equipment (RPE) are vital for frontline health workers that work with patients infected with contagious respiratory tract infections, such as the coronavirus disease 2019 (COVID-19). During the early pandemic, there was an exceptionally high global demand for RPE but supply chains were under severe strain and supply continuity remained uncertain. There is a constant demand for RPE masks as they are disposable items or have a short lifetime as the filters need to be replaced or decontaminated after prolonged use, which could damage

the integrity of the fibers and remove their electrostatic charge. Additive manufacturing (AM) has been widely utilized for various applications, such as in the fields of aerospace<sup>[1]</sup>, automobiles<sup>[2]</sup>, and tissue engineering<sup>[3]</sup>, and now, the AM community has developed three-dimensional (3D) printing initiatives to support health care and frontline workers<sup>[4]</sup>. This includes rapid printable face shields for health care workers that can reduce direct exposure from large airborne respiratory droplets<sup>[5]</sup>. However, these initiatives are limited by the material choice and technology that produces masks for respiratory protection. A key component of RPE is the filtering mechanism. The filter traps and retains airborne

© 2021 Sherborne and Claeyssens. This is an Open Access article distributed under the terms of the Creative Commons Attribution-NonCommercial 4.0 International License (<http://creativecommons.org/licenses/by-nc/4.0/>), permitting all non-commercial use, distribution, and reproduction in any medium, provided the original work is properly cited.

Please cite this article as: Sherborne C, Claeyssens F, 2021, Considerations using additive manufacture of emulsion inks to produce respiratory protective filters against viral respiratory tract infections such as the COVID-19 virus. *Int J Bioprint*. DOI: 10.18063/ijb.v7i1.316

contaminants, such as virus-laden aerosol particles, while letting air pass through.

This review presents the feasibility of a polymerized high internal phase emulsion (polyHIPE)-based filter, and whether current emulsion-based AM techniques can be used to produce RPE against COVID-19. The motivation behind AM to make a porous foam is that it can produce complex geometries. The advantages include a multimaterial filter, localized and functionalized surface, or tunable porosity gradients to control the airflow within the filter itself. This approach could facilitate new filter designs that capitalize on new material processing and manufacturing techniques that may overcome some limitations of fibrous filters. Furthermore, the new filter designs may potentially filter the most penetrating particle size of 0.3  $\mu\text{m}$ , which is the most difficult to filter because this size is at the transition point between particles that predominantly move by Brownian motion and larger particles that move by straight trajectory. This review provides an overview of the current filter-based applications of emulsion templating, including the current state of emulsion ink-based AM and the European Standard (EN) guidelines regarding the requirements of a RPE filter.

In this review, the following considerations are covered:

- RPE requirements including ISO standards and regulations that a new filter material will need to comply with;
- An overview of the polyHIPE material, current filter, and separation-based applications;
- AM of polyHIPE foams, their advantages, limitations, and the current progress in the literature to 3D printing using emulsions.

## 2. Respiratory filter requirements for COVID-19 prevention

RPE is a broad term covering respirators or breathing apparatus that filter or remove harmful substances from the air we breathe. For health care workers, different RPE types are recommended depending on the exposure risk from the COVID-19 patients<sup>[6]</sup>. Furthermore, government guidelines are in place for infection prevention<sup>[7]</sup>. The size of severe acute respiratory syndrome coronavirus-2 that causes COVID-19 is between 50 and 200 nm wide<sup>[8]</sup>. COVID-19 is thought to transmit through close contact and contaminated droplets over short distances<sup>[9]</sup>. When an infected patient coughs or sneezes, large airborne respiratory droplets laden with the virus are produced, contaminating surfaces and potentially transmitting the virus to others nearby. Hence, wearing a face mask is able to protect the surrounding people from respiratory droplets. Two-meter social distancing, frequent hand washing, and usage of mouth coverings/face mask are approaches

to prevent the transmission. It is widely accepted that mask wearing could reduce COVID-19 transmission as it provides continuous protection from the contamination from the respiratory droplets and acts as a barrier to stop direct contacts of hands to mouth, nose, or eyes<sup>[10]</sup>. There is high certainty that the inhalation of the virus-containing aerosols is one of the infection modes, as determined by computer modeling of speech and cough that generated droplets from infected individuals<sup>[11]</sup>. Nevertheless, this is largely dependent on the respiratory droplets that suspend in the air for a certain period of time.

The health care workers are at a great risk of infection when using aerosol-generating procedures on COVID-19 patients<sup>[6]</sup> as these airway-based procedures can create fine particles of <5  $\mu\text{m}$  which can remain suspended in the air. For example, procedures such as tracheal intubation and non-invasive ventilation can produce virus-laden particles of smaller than 10  $\mu\text{m}$ , which are very likely to bypass the respiratory mucosa in the upper airways and penetrate deep into the lung, thereby increasing the infection risk<sup>[12]</sup>. The World Health Organization recommends having adequate supply of PPE, such as N95 respirators, filtering facepieces (FFP3 or FFP2), or their equivalents, as part of the RPE<sup>[9]</sup>.

Several ways the airborne particles can deposit onto the fibers include impaction, interception, and electrostatic forces. To improve breathability, the respirators must be permeable to air while maintaining their particle filtering function. To achieve this, the fibers have electrostatic charge to attract and trap airborne particles that attach onto the fiber<sup>[13]</sup>. Sterilizing these filters using ethanol<sup>[14]</sup> or isopropanol<sup>[15]</sup> removes the electric charge from the fibers which reduces their effectiveness.

According to the US National Institute for Occupational Safety and Health, N95 masks that can filter at least 95% of the airborne particles use an electrostatically charged non-woven polypropylene (PP) fiber to filter out airborne particles. The protective feature of these masks is comparable to that of the European FFP2 filters. In future, the masks should be designed in a way to include a seal around the face to prevent the bypass of submicron particles through the filter mechanism, which can occur during head movements<sup>[16]</sup>. 3D printing is a potential solution as it can be combined with detailed face scans to produce a customized face seal for improved wearer comfort and fit<sup>[17]</sup>. A customized 3D-printed reusable facemask with a replaceable filter membrane has been proposed<sup>[18]</sup>. FFP2/3 filter membranes can be used as a replaceable part of the mask.

## 3. RPE regulations

There are three classes of respiratory filters: FFP1, FFP2, and FFP3. A higher grade indicates a better filter efficiency; FFP3 can filter out at least 99% of airborne

particulates. During classification, the respirators are tested to certify whether they conform to the British or European standard (BS) EN 149:2001+A1:2009<sup>[19]</sup>. The “Conformité Européen” (CE) marking affixed to the PPE is an evidence of compliance to this legislation and an indication of the effectiveness of the respirator. A selection of these requirements is summarized in **Table 1**. In the United Kingdom, the HSG53 (2013) is a guideline recommending the best industry practice for the usage of RPE and its standard requirement. FFP3 is recommended in clinical use for protection against biological agents, including pandemic flu. Comparison tests between FFP3, FFP2, FFP1, and surgical masks show that there is a gradual decrease in the protection level with surgical masks offering the lowest level as they do not seal around the face<sup>[20]</sup>. Performance testing showed that the FFP2 and FFP3 masks achieved <1% and <0.03% for the penetration of polydisperse sodium chloride (NaCl) aerosols with a MMD (mass median diameter) of 238 nm, respectively<sup>[15]</sup>. Surgical masks offer some protection against the large droplets and contact transmission so symptomatic patients should wear it to minimize the spread of respiratory secretions that could transmit the infection to the surrounding. Respirators with a tight face seal are recommended over masks for enhanced protection. In regard to 3D-printed PPE-related devices from the 3D printing community, care should be taken when using them, as the devices are not approved by the relevant regulatory bodies for clinical use and their effectiveness is not guaranteed. Therefore, these devices should be used at the user’s discretion.

The assigned protection factor indicates the level of protection that could be provided by the respirator (**Table 1**). A protection factor of 10 means that the user particle exposure level is reduced by a factor of 10, so one-tenth of the air contaminants will be breathed in. FFP3 is considered to be twice as effective as FFP2. All respirators require a tight-fitting face seal otherwise particles can bypass the filter through the open gaps. The total permitted inward leakage accounts for all potential leakage paths around the filter when the face seal leaks<sup>[21]</sup>.

Furthermore, any PPE or RPE for the European market has to meet the required health and safety

requirements of the European Directive on PPE Regulation (EU) 2016/425. This covers the legal obligations to ensure that the manufacture of PPE meets the required standards relating to the design, manufacture, and marketing of PPE. Furthermore, commission recommendation (EU) 2020/403 was introduced recently during the COVID-19 crisis to speed up the delivery of PPE to the market, specifically for the medical professionals.

#### 4. Overview of the polyHIPE

PolyHIPE is a porous polymer that is created by polymerizing the continuous phase of an emulsion where the droplet phase exceeds over 74% of the total liquid volume; this type of emulsion is called a high internal phase emulsion (HIPE). The two liquids have to be immiscible with each other; therefore, when they are mixed together with either a surfactant or a small pickering particle, one of the liquids is broken into droplets (droplet phase) that disperse within the other (continuous phase). A polymeric material known as a polyHIPE is created when the emulsion’s continuous phase is set into a solid. This can be done using either a light<sup>[22]</sup>, heat<sup>[23]</sup>, or a redox-based polymerization reaction<sup>[24]</sup>. During the crosslinking, the 3D architecture of the emulsion’s continuous phase is fixed as a solid polymer, and subsequently, the draining of the droplet phase leaves behind a porous polymer. A unique property of the polyHIPE is that the porosity parameters can be independently tuned through the initial emulsion mixing conditions and ingredients. These include physical parameters, such as temperature<sup>[23]</sup>, speed of mixing<sup>[25-27]</sup>, and the rate the droplet phase is added<sup>[28]</sup>. The emulsion constituents can be varied from different aspects, such as water volume ratio<sup>[29]</sup>, monomer type<sup>[30,31]</sup>, solvent used in the emulsion<sup>[32,33]</sup>, amount of surfactant<sup>[34]</sup>, surfactant-free pickering emulsion<sup>[35]</sup>, solubility of the initiator<sup>[36]</sup>, and addition of electrolytes to the droplet phase<sup>[31]</sup>. These variables affect the stability of emulsion, the droplet size, and the way the monomer polymerizes around the droplets. A representative scanning electron microscope image of the polyHIPE structure is shown in **Figure 1**.

During the polymerization, the monomers cross-link to form a polymer chain. This process coincides with a significant volume reduction or contraction.

**Table 1.** Classification requirements of FFP1, FFP2, and FFP3 respirators

| Classification | Protection factor | Max. penetration of test aerosol:<br>95 l/min max % |              | Max. permitted<br>resistance (mbar) |                         | Total permitted<br>inward leakage<br>(%) |
|----------------|-------------------|---|--------------|-------------------------------------|-------------------------|--|
|                |                   | Sodium chloride                                     | Paraffin oil | Inhalation<br>30/l min              | Exhalation<br>160 l/min |  |
|                |                   |   |              |                                     |                         |  |
| FFP1           | 4                 | 20  | 20           | 0.6                                 | 3                       | 25                                       |
| FFP2           | 10                | 6   | 6            | 0.7                                 | 3                       | 11                                       |
| FFP3           | 20                | 1   | 1            | 1                                   | 3                       | 5  |

Information adapted from the British standard: BS EN 149:2001+A1:2009<sup>[19]</sup>. FFP, filtering facepieces.

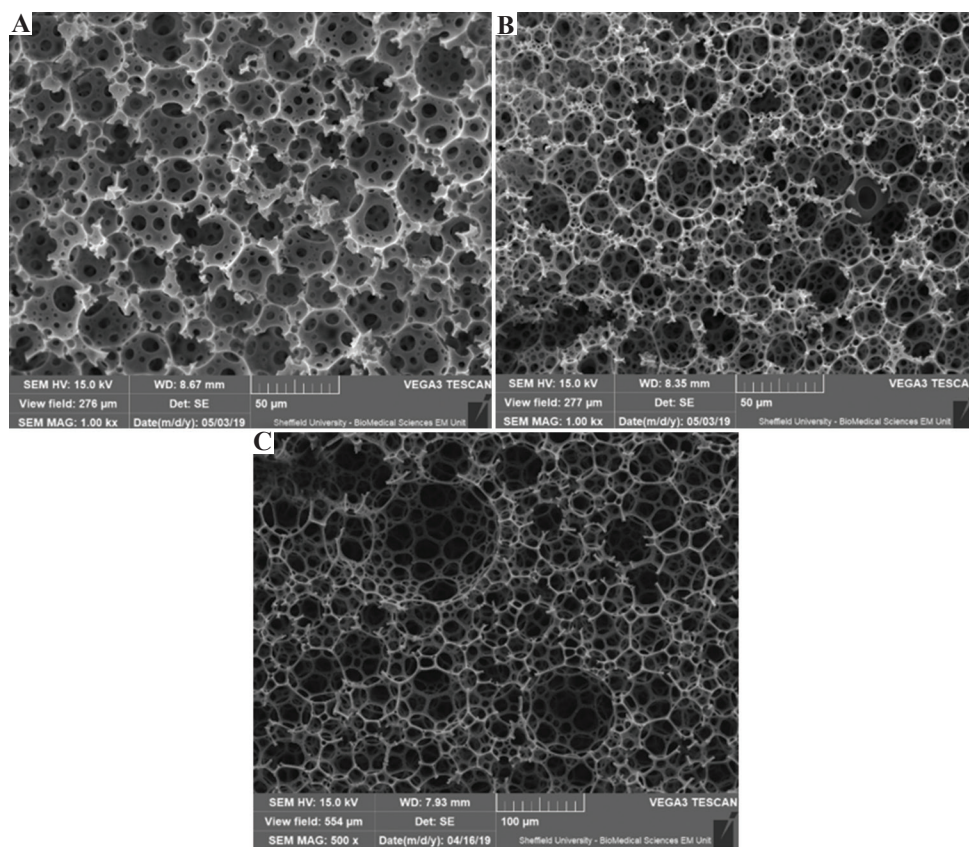


**Figure 1.** Scanning electron microscope pictures showing an example of the polymerized high internal phase emulsions structure made with different water ratios. The monomer-to-water ratios are (A) 1:9, (B) 1:20, and (C) 1:40. All samples contain 10 wt% surfactant relative to the monomer and were mixed at 350 rpm.

This is because the distance between the monomers reduces from a typical van der Waals distance ( $\sim 3$  Å) to a covalent bond distance ( $\sim 1.54$  Å) during polymerization. This contraction creates interconnecting windows (holes) between adjacent water droplets<sup>[37]</sup>. In the HIPE emulsion, tightly packed water droplets deform into polyhedral shapes<sup>[38]</sup>. A thin coating of monomer and surfactant prevents them from merging together. This barrier ruptures and breaks apart during the polymerization reaction to create the connecting windows. Monomers such as methyl acrylate have a high contraction level during polymerization, and varying its amount in the emulsion can modify the interconnectivity<sup>[30]</sup>. Furthermore, increasing the water volume ratio in the initial emulsion increases porosity and openness by creating a thinner monomer film surrounding water droplets<sup>[39]</sup>.

The surfactant has a profound effect on emulsion stability and directly affects the polyHIPE interconnectivity, permeability, and size of the pores in the polymer structure<sup>[40]</sup>. A surfactant with a concentration below 5 wt% relative to the monomer in the initial emulsion creates a polyHIPE with closed porosity, up to 10 wt% creates small connecting windows which

increase until around 45 wt%; an amount higher than this will cause a gradual decline in the physical properties and structural collapse<sup>[34]</sup>. The surfactant is an amphiphilic compound which stabilizes the emulsion by orientating itself at the interface between the two emulsion phases with the hydrophobic part pointed toward the oil phase and the hydrophilic head group toward the aqueous phase<sup>[41]</sup>. Surfactants are classified by their hydrophilic-lipophilic balance (HLB) number which relates to the ratio between the hydrophilic and the lipophilic parts of the surfactant; low HLB (3–6) is oil soluble and used for water droplets in oil (W/O) emulsions, whereas high HLB (8–18) is water soluble for O/W emulsions<sup>[41]</sup>. A stable emulsion can accommodate a thin barrier film between adjacent water droplets, which is more prone to rupture during polymerization.

Filter-based applications may require small pore sizes and high surface area. This can be achieved by either an increase in the surfactant or addition of a salt to the emulsions droplet phase, as shown comprehensively by Williams *et al.*<sup>[31]</sup> Typical polyHIPEs have a surface area around  $3\text{--}20\text{ m}^2\text{g}^{-1}$ , but replacing some monomeric continuous phase with a solvent can increase the area to  $829\text{ m}^2\text{g}^{-1}$  depending on the solvent used<sup>[33]</sup>. Solvents in

the continuous phase can act as a cosurfactant that results in smaller pores and an increased interconnectivity between the pores<sup>[32]</sup>.

There is a range of research interest in emulsion templating to create porous polyHIPE structures<sup>[42-46]</sup>. The research interest also extends to their potential for a range of fluid separation applications, including filters, membranes, and chromatography<sup>[47]</sup>. There are detailed reviews on emulsion templating applications<sup>[48-51]</sup> as well as the range of materials and uses of a porous foam manufactured using both liquid- and bubble-based templating<sup>[52]</sup>. Some specific reviews also detailed the porous materials and uses of HIPE-based emulsions and foam templating<sup>[53]</sup> as well as the potential of 3D printing as a method to produce tissue engineering scaffolds<sup>[54]</sup>.

## 5. Considerations for a polyHIPE-based RPE filter against viruses

The perspective polyHIPE filters need to be tested to determine its effectiveness as a RPE filter in relation to different porosities, thicknesses, and surface functionalization. The average inhalation under moderate and strenuous workload 30 L/min and 85 L/min, respectively<sup>[14]</sup>. To test the filter efficiency under these flow rates, typically NaCl particles are aerosolized using a particle generator and the particle concentration is tested up- and downstream of the filter. This testing can also represent aerosolized single viruses using small, 0.037–3.2  $\mu\text{m}$ , sized particles<sup>[14]</sup>.

The porosity, chemical functionality, and mechanical strength of the polyHIPE can be independently tuned based on the emulsion constituents or conditions. This adjustment has led to a variety of separation-based applications, including filter, metal ion separation, and chromatography<sup>[55]</sup>. PolyHIPEs have a huge separation potential with a tunable permeability, an ability to alter surface chemistry, different material choices, and interconnected pores; their uses as a filter for small molecule separation have been reviewed<sup>[56]</sup>.

The requirements of polyHIPE specifically for the production of a respirator filter that can prevent the transmission of aerosolized virus-laden particles have yet to be defined. In the aspect of virus filtration, there is a difference between mechanical filtration (pore size/interconnectivity) and the use of an optimally functionalized surface for immobilizing the virus onto the polymer. Despite lacking the information regarding the pore size, an example of virus filtration elaborated in the withdrawn 2008 patent EP 1 889 811 A1 highlights the importance of a functionalized surface (aminated, sulfonated, or betainated) to improve the filtration of poliovirus type 1 from water. The presented data showed the removal of 99.99%

poliovirus through a functionalized surface against the 99% reduction in a non-functionalized one. The filter could also be regenerated using either a concentrated electrolyte/acidic or alkaline solution depending on the surface functionalization. A heparin-coated polyHIPE-based chromatographic column has also been used to selectively bind *Enterovirus 71* and purify it from solutions, and the polyHIPE has a porosity of 0.2–0.5  $\mu\text{m}$  and interconnected pore sizes in the range of 0.5–2  $\mu\text{m}$  for the isolation of virus particles<sup>[57]</sup>. The virus can be eluted from the column afterward.

Infection by airborne transmission occurs after the inhalation of the contaminated droplets. Aerosol transmission of virus-laden droplets is still not fully understood in terms of the effects of the exhaled particle size distribution and the number of infectious viruses in each particle<sup>[11]</sup>. The virus itself is between 50 and 200 nm in radius. Typical speech and coughing can produce aerosolized liquid droplets with an average size of <20  $\mu\text{m}$  which could linger in the air between 20 min and 1 h depending on the environmental conditions; 50 and 100  $\mu\text{m}$  sized particles can stay in the air for approximately 20 s and 3 min while smaller particles can potentially remain airborne for a longer period of time. Nevertheless, all particles pose a potential risk of being inhaled while they remain airborne. It is important to note that the chances of inhalation increase as the particle size reduces<sup>[11]</sup>.

The principal function of a majority of the polyHIPE-based air filters is to remove particulates from the air. Vehicle exhaust fumes represent a major source of air pollution, for example, the hydrocarbon fragments produced from the partial combustion of fuel<sup>[58]</sup>. In particular, there is a need to filter out airborne particulate matter of <2.5  $\mu\text{m}$  ( $\text{PM}_{2.5}$ ) as these particles in this size range can damage the respiratory system<sup>[59]</sup>. According to the ISO standardized vocabulary for ultrafine particulate matter (PM),  $\text{PM}_{0.1}$  refers to the particulates with aerodynamic diameters of 100 nm or less,  $\text{PM}_{2.5}$  with 2.5  $\mu\text{m}$ , and  $\text{PM}_{10}$  with 10  $\mu\text{m}$ <sup>[60]</sup>. Small pollutants of <2.5  $\mu\text{m}$  are small enough to penetrate deep into the lungs and cause damage to the alveolar walls.

A polyHIPE-based aerosol filter for automobile exhaust achieved an increase in the capture efficiency of particles (<2.5  $\mu\text{m}$ ) from 1.2% to 72.2% after surface functionalisation of an amino ( $-\text{NH}_2$ ) end group<sup>[61]</sup>. The polyHIPE filter captured these particles both on the outer surface and within the pores (pore sizes were between 3.0 and 7.4  $\mu\text{m}$ , interconnects of 1.1 and 2.4  $\mu\text{m}$ ), and its effectiveness was attributed to the surface coating as well as the coating thickness physically reducing the interconnect and pore size. The filtering efficiency of a sample with a thickness between 1 and 14 mm rose from 65 to 80% in filtering particulates of <2.5  $\mu\text{m}$ .

This highlights that in addition to sample thickness, other factors, such as porosity and interconnectivity of the polyHIPE, are also required for improving filtering efficiency.

There is trade-off between the polyHIPE pore size/interconnectivity and the air flow resistance through the material. Smaller pores not only increase the strength of filtration but also the air flow resistance, which is recorded as an increased pressure drop<sup>[62]</sup>. A more permeable filter will have a lower pressure drop, but at a cost of filtration efficiency. This is the same for fibrous masks in which the air flow is typically perpendicular to the packed fibres. Increasing the amount of fibrous material improves particle capture, but causes more air flow resistance<sup>[63]</sup>. Ideally, the filter should have a low pressure drop and high collection efficiency<sup>[13]</sup>. Typical filters are porous materials that allow air transfer while trapping airborne particles; there are several types of trapping mechanisms<sup>[13]</sup>. A typical filter example is Nylon6 (N6)-based non-woven fibrous mesh made by electrospinning<sup>[63]</sup>.

## 6. PolyHIPE filter applications

To create micron-sized pores within the polyHIPE, the initial emulsion can be mixed using a high-speed homogenizer (25,000 rpm), resulting in average pore diameters between 0.6 and 4.5  $\mu\text{m}$ , an increase in interconnectivity was observed when increasing the surfactant from 5 to 15wt%, and the porosity from 75 to 90%<sup>[27]</sup>. A styrene/divinylbenzene (St-DVB)-based fibrous polyHIPE with pore sizes ranging from 2 to 7  $\mu\text{m}$  and interconnect windows down to 1  $\mu\text{m}$  was produced by tuning both the surfactant and mixing methods<sup>[29]</sup>.

The polyHIPE structure has been used for the chromatographic separation of proteins because of its tunable porosity and flexible polymer choice. Glycidyl methacrylate (GMA) is a popular monomer for this application because it can be chemically functionalized through the epoxy groups<sup>[64]</sup>. A list can be found in **Table 2**. When used with the cross-linker ethylene glycol dimethacrylate (EGDMA), polyHIPEs created from these monomers are more hydrophilic compared to their styrene/DVB counterparts. Poly(GMA-co-EGDMA)-based polyHIPEs have been reported to have 1–10  $\mu\text{m}$  pores with submicron interconnects for protein separation<sup>[64]</sup>. They can be blended with an elastomer chemically modified with diethylamine to get weak anion exchange supports in the flexible membrane for protein purification by ion exchange chromatography with 3–10  $\mu\text{m}$  porosity and 1–3  $\mu\text{m}$  interconnects<sup>[65]</sup>. A similar polyHIPE polymer blend has been continuously reused over 300 times<sup>[66]</sup>, and grafted GMA brushes have been used for chromatographic separation of proteins in an epoxy-based monoliths<sup>[67]</sup>.

A redox-initiated polymerization of a poly(methyl methacrylate)-based polyHIPE filter can be cured *in situ* within a tubular mold and used within 20 min. This is useful if the housing material is opaque to light or heat sensitive as the reaction can occur at room temperature<sup>[24]</sup>. A similar polymerization method has been used for the polyHIPE-based chromatography protein purification<sup>[65]</sup>. Low porosity emulsion templated foams still retain some permeability<sup>[40]</sup>, but it lacks the interconnectivity level obtained using high volumes of water in the initial emulsion.

PolyHIPEs created from a W/O emulsion are hydrophobic because a water immiscible monomer is used in the initial emulsion. This hydrophobicity has led to applications such as oil or organic solvent removal from water where recycled polystyrene is one of the monomers<sup>[68]</sup>. Hydrophobicity can be increased by adding  $\text{Fe}_3\text{O}_4$  to the initial monomer to create superhydrophobic foams (contact angle over 150°) to remove oil or organic solvent pollutants from water<sup>[69]</sup>. A poly(dicyclopentadiene)-based polyHIPE oxidizes in air to produce reactive peroxy species that can be used to either decontaminate nerve agents<sup>[70]</sup> or produce a self-decontaminating air filter<sup>[71]</sup>.

A poly(styrene-co-DVB) polyHIPE column with mean interconnects 0.57–0.59  $\mu\text{m}$  can separate 52 nm particles from 155 nm ones through a difference in retention time<sup>[72]</sup>. For other aqueous-based filter applications, the surface of the polyHIPE can be sulfonated to create a more hydrophilic surface and subsequently used to filter 1–11  $\mu\text{m}$  particles of calcium carbonate (aragonite) dispersed in water<sup>[73]</sup>. For microfiltration applications, the outer surface of polyHIPEs can also be functionalized *in situ* by adding a hydrophilic monomer, such as sodium acrylate, to the emulsion droplet phase to filter out microalgae<sup>[74]</sup>. PolyHIPE scaffolds coated with iron hydroxides can remove arsenic from contaminated water<sup>[75]</sup>. The use of pickering based polyHIPEs for the decontamination of pollutants water has been reviewed in detail elsewhere<sup>[76]</sup>.

To create a simple polyHIPE sheet, an open pored surface is critical and care is needed to maintain the surface porosity when curing the HIPE into a mold to create a porous membrane. The use of either a hydrophilic or hydrophobic mold material affects the surface porosity of the polyHIPE at the HIPE/mold interface<sup>[43,73,77-80]</sup>. An open or closed pored surface is created by preferential wetting of the mold surface with either the aqueous or monomeric (oil) phase of the HIPE and is postulated to relate to the surfactant orientation at the mold surface<sup>[73]</sup>. When polymerizing a W/O emulsions such as St-DVB in water, the emulsion can destabilize against a PVC mold, have a closed pored surface skin against a PP mold and an open porosity against a PTFE one<sup>[43]</sup>. The amount of open surface porosity can be fine-tuned by varying the

**Table 2.** PolyHIPE filter-based applications

| Material  | Application   | Pore size (µm)     | Interconnect (µm) | Surface functionalization  | Characteristics   | Ref     |
|---|---|--------------------|-------------------|--|---|---------|
| Poly(St-MMA-DVB)  | Air filter  | 3.0–7.4            | 1.1–2.4           | Amino (–NH <sub>2</sub> ) functionalized   | High thermal resistance   | [61]    |
| Poly(St-GMA-DVB)  | Column to purify virus for vaccine production                                 | 0.5–2              | 0.2–0.5           | Heparin  | Heparin functionalized to purify <i>Enterovirus 71</i> (EV71)                                   | [57]    |
| PEGMA-SA-PEGDA  | 3D-printed hemostatic and absorbent polyHIPE wound dressing                   | ≈3                 | ≈0.75             | -  | Kaolin-loaded, 3D-printed cure on dispense 3D printed   | [87]    |
| Poly(GMA -EGDMA)  | Protein separation through chromatography                                     | 1–10               | 0.1–0.5           | Modified to bear weak anion exchange groups  | Surface epoxy groups can be chemically modified   | [64]    |
| Poly(GMA -EGDMA-EHA)                                    | Protein purification by chromatography  | 3 – 10             | 1 – 3             | Surface functionalized to create weak anion exchange supports                        | Flexible polyHIPE membranes that can be rolled into a module                                    | [65]    |
| Epoxy resin-based monolith with GMA brushes             | Ion exchange chromatography   | -                  | -                 | Anion exchange functionality using iodomethane                                       | Proteins recovery with no obvious sign of unfolding   | [67]    |
| Poly(GMA -co-EGDMA)                                     | Protein separation by chromatography  | 0.6–0.1            | -                 | Surface modified by diethylamine   | High column efficiency and protein-binding capacity   | [66]    |
| Poly(MMA-co-EGDMA) and poly(BeMa-co-EGDMA)              | <i>In situ</i> cured open pored filter  | 16–29              | 2.4–6.4           | -  | Redox-initiated polymerization for <i>in situ</i> polymerization of a filter                    | [24]    |
| Sulfonated polystyrene, EGDMA, TEOS, and butyl acrylate | Oil recovery  | 82.3–145.6         | 7.8–13.5          | -  | Made using recycled polystyrene   | [68]    |
| Poly(St-DVB)  | Oil spill recovery  | -                  | -                 | -  | Fe <sub>3</sub> O <sub>4</sub> increased hydrophobicity   | [69]    |
| Poly(DCPD)  | Decontamination of chemical warfare agent and self-decontaminating air filter | 1–4                | -                 | Air oxidation produces hydroperoxide species   | Rapidly oxidizes at 85°C; decontaminates chemical warfare agents                                | [70,71] |
| Poly(St-DVB) with EHA or ethyl vinyl benzene            | Microfiltration   | 23.9±16.4          | -                 | Sulfonated to produce hydrophilic surface  | Filtration of 1–11 µm particles of calcium carbonate in water                                   | [73]    |
| Poly(St-DVB) and poly(EGDMA)                            | Chromatographic separation of nanoparticles                                   | 1.08–1.12          | 0.19–0.59         | -  | Separation of engineered nanoparticles (52 nm, 155 nm)  | [72]    |
| Poly(butyl acrylate- EGDMA)                             | Ultrafiltration of microalgae   | 1–80               | 0.1–3             | <i>In situ</i> functionalization using sodium acrylate                               | Hydrophilic surface through <i>in situ</i> functionalization                                    | [74]    |
| Poly(St-b -P4VP)  | Bacteria filter and its inactivation using NIR sterilization                  | 5–50               | 1–5               | Stabilized with amphiphilic block copolymers for potential surface functionalization | Coating with polypyrrole nanoparticles and NIR-induced heat to sterilize (20–180°C) within 10 s | [82]    |
| Poly(MMA-EGDMA)   | Improved mechanical properties of polyHIPE                                    | 0.8–25 and 0.6–4.5 | 0.2–5.9           | -  | High E-moduli up to 211 MPa   | [27]    |
| Poly(St-DVB)  | Ultra-low-density polyHIPE  | 1.6–9.3            | -                 | -  | Ultra-low-density achieved 0.0126 g/cm <sup>3</sup>   | [29]    |

The monomer abbreviations used are: MMA, methyl methacrylate; EGDMA, ethylene glycol dimethacrylate, DVB, divinylbenzene; GMA, glycidyl methacrylate; EHA, ethylhexyl acrylate; BeMA, benzyl methacrylate, TEOS, tetraethyl orthosilicate; St, styrene; DCPD, dicyclopentadiene, P4VP, polyvinylpyridine; PEG, polyethylene glycol; SA, sodium acrylate; PEGDA, polyethylene glycol diacrylate; PEGMA, polyethylene glycol methacrylate.



surfactant amount and droplet volume ratio of the initial emulsion<sup>[77]</sup>. A hydrophilic material is required to create an open surface with W/O emulsions. This can include hydrophilic glass surface<sup>[78-80]</sup> or alginate<sup>[81]</sup>.

PolyHIPE-based bacteria filters can be surface-coated with polypyrrole nanoparticles. These particles act as nanoheater that can be heated to 180°C within 10 s using near-infrared irradiation to kill trapped bacteria<sup>[82]</sup>. An approach like this could be beneficial for sterilizing a polyHIPE-based filter as the inner surface of current N95 filters can have a warm, wet microclimate which can contribute to bacterial growth (a strategy that could also work for viral infections)<sup>[83]</sup>. Silver is an effective antibacterial agent and can be coated on the surface of a polystyrene sulfonate-based polyHIPE<sup>[84]</sup> or a polystyrene-based polyHIPE<sup>[85]</sup>. Alternatively, broad-spectrum antimicrobial activity can be obtained by iodine-releasing polyHIPEs made from kaolin-containing cross-linked PEG-NaAA-PEG polyHIPEs<sup>[86]</sup>. These can be 3D printed into a mesh for wound dressing<sup>[87]</sup> as iodine is both antimicrobial and virucidal<sup>[88]</sup>. Alternatively, antibacterial properties of the polyHIPE surface can be acquired by dipping the polymer in antibiotics, such as ciprofloxacin or tetracycline HCL, although freezing and lyophilizing are required afterward as reported in this case<sup>[89]</sup>. However, antibiotics do not work against viral infections.

Electrospinning has also been combined with emulsion templating to prevent cell migration in a tissue engineered scaffold<sup>[90]</sup>. This hybrid manufacture approach has the potential to combine the strengths of fibrous and emulsion templated porous structures. Nanofibrous-based emulsion templated foams are fragile and can be difficult to scale. Nanofibrous porous syndiotactic polystyrene-based polyHIPE (average fibrous diameter of about 24 nm) can be used to remove airborne volatile organic compounds; however, the reported manufacture method required extensive extraction through boiling in acetone and freeze-drying to produce the structures according to the choice of material<sup>[91]</sup>.

## 7. AM of emulsions

Emulsions, in particular, HIPEs that contain photocurable monomer can be used as an ink for AM techniques. Stereolithography and extrusion-based printing are 3D printing techniques that can be used to print with these emulsions. The conditions of the emulsion used in these techniques can control the porosity, while the print design determines the bulk shape. The HIPE viscosity can be tailored for each technique: low speed mixing (350rpm) creates a liquid suitable for stereolithography<sup>[92]</sup>. While, a highly viscous emulsion is advantageous for its shape retention during extrusion-based 3D printing. This can be achieved either through additives<sup>[93]</sup>, high-speed mixing (2500 rpm) [94], or other methods to change the

viscosity<sup>[95]</sup>. Since the emulsion is a liquid, its benefits and constraints are similar to those of the liquid-based 3D printing<sup>[96]</sup>. A review of the current progress of AM coupled with emulsion templating is discussed below.

## 8. Stereolithography of HIPE

Raster scanning UV laser light across the top surface of a vat of HIPE can be used to polymerize both simple porous polyHIPE shapes on top of a glass surface using an in-house built microstereolithography ( $\mu$ SL) rig<sup>[92]</sup>. Later, the group produced a woodpile structure of alternative polyHIPE lines of 350  $\mu$ m and used it as a porous scaffold for tissue culture support<sup>[39,97,98]</sup> (**Figure 2**). The size of the polymerized regions varied with write speed and UV light power, and the droplet size determines the achievable minimum feature size. The internal microporosity of the 3D-printed polyHIPE was preserved and comparable to a bulk cured emulsion.

Light-based raster scanning of HIPEs requires careful control over light scattering to reduce both the overcuring and formation of a surface skin on the polyHIPE<sup>[99]</sup>. The refractive index mismatches between the water and oil phase scatters light, and this results in the characteristic whiteness of the emulsion. This effect is problematic during stereolithography as the emulsion also scatters the polymerizing light outward from the point of exposure, creating a gradually reduced cross-linked monomer gradient that decreases outward from polymerized polymer to liquid monomer. On washing, this partially polymerized polymer collapses on itself, covering the polyHIPE with a surface skin. Overlapping of two partially polymerized regions fully polymerizes the polymer causing overcuring and connecting polymer bridges<sup>[99]</sup>. To reduce the surface skin and increase printable resolution, a light absorber can be used to control the light scattering<sup>[99]</sup>. A surface skin is also found when the HIPE is polymerized against certain mold materials.<sup>[43,73,77-80]</sup> Although a closed, pored outer surface can act as a barrier to slow down drug release from a 3D-printed emulsion-based hydrogel<sup>[100]</sup>, it is detrimental for filter-based applications.

A dynamic mask projection-based stereolithography approach can be used to 3D print the HIPE ink using a digital micromirror device (DMD) to produce complex 3D shapes in a layer-by-layer fashion<sup>[101]</sup>. A light absorber is still required to improve resolution, and the authors did not mention whether there was an outer surface skin. The authors reported that this layer-by-layer-based printing is sensitive to viscosity of the emulsion, which can be lowered using a solvent such as toluene. Furthermore, DMD projection can be used to 3D print porous polyHIPE tubes in a continuous process<sup>[92]</sup>. A functional polymer-based polyHIPE made of GMA was 3D printed using a digital light processing (DLP) printer to create

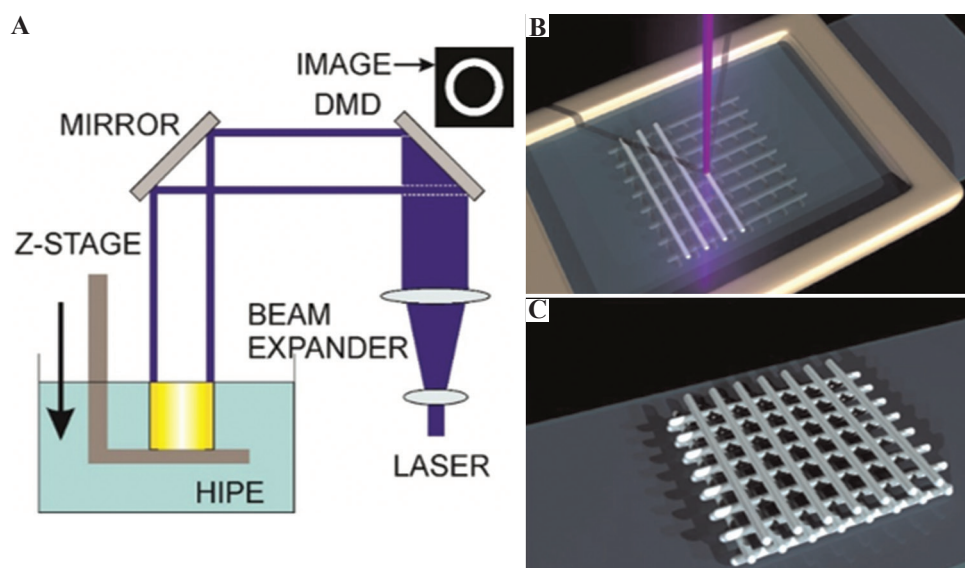


**Figure 2.** Schematic (A) and 3D rendering (B and C) showing a projection and raster scanning-based 3D printing. (A) reproduced from Ref.<sup>[92]</sup> with permission from John Wiley and Sons, Licensed under Creative Common License. (B) and (C) modified from Journal of the Mechanical Behavior of Biomedical Materials, Volume 54, Owen R, Sherbone C, Paterson T, *et al.* Emulsion templated scaffolds with tunable mechanical properties for bone tissue engineering, pp 159-172, Copyright (2016), with permission from Elsevier<sup>[39]</sup>.

a chromatography column<sup>[102]</sup>. Other DLP-based 3D printing techniques have used an oil-in-water emulsion-based ink consisting of droplets of photocurable ink within an aqueous suspension<sup>[103]</sup>.

The 3D print speeds vary depending on the method used. The single line writing speeds of direct laser writing for printing polyHIPE are 1 – 5 mm/s, which is dependent on the laser power<sup>[92]</sup>. With these speeds the authors created a circular 13mm, 4 layered woodpile structure in 13 minutes<sup>[39]</sup>. Alternatively, the projection-based stereolithography can print a 17.25 mm<sup>2</sup> surface area and complex geometries simultaneously at a printing speed of 2 vertical mm/h<sup>-1</sup> for a layer thickness of 25 μm<sup>[101]</sup>. Stereolithography-based 3D printing setups are becoming quite cost effective, after the major patent protecting the technique (US5762856A, Hull) expired in 2015 and start-up companies started to produce low-cost setups.

## 9. Extrusion-based 3D printing

Through a manufacturing process known as material extrusion (also called fused deposition modeling or robocasting), a HIPE ink can be extruded through a syringe and polymerized using UV light to create a porous polyHIPE-based structure (**Figure 3**). High emulsion viscosity is suitable for this 3D printing method as the emulsion ink can maintain its structure post-extrusion without unwanted spreading before polymerization, and the emulsion viscosity is tunable by altering the respective component amounts in the emulsion<sup>[93]</sup>. No surface skin is observed on the outer surface of extrusion-based 3D-printed polyHIPEs<sup>[93]</sup>. This is expected as

the emulsion is curing against air; therefore, there is no surface contact with a material that can adversely affect the surface porosity by surface destabilization. This technique has also been used to create a composite polyHIPE for use as a biocatalytic flow reactor using an enzyme-laden hydrogel as the emulsion droplet phase<sup>[104]</sup>. Alternatively, an emulsion can simply be injected directly into a void before bulk polymerization<sup>[25]</sup>. Extrusion-based printing of emulsion has been demonstrated to print at a speed of 10 mm s<sup>-1</sup> with extrusion width of 0.6 mm using a modified RepRap style 3D printer<sup>[93]</sup>. Modified extrusion-based 3D printers have been used to print emulsions that are cured on demand, with print speeds tested up to 9 mm/s and layer heights of 100–300 μm<sup>[104]</sup>.

To create hydrophilic porous foams through material extrusion, an oil-in-water emulsion can be used with a UV cure during extrusion. Some of the materials include poly(ethylene glycol) diacrylate (PEGDA), alginate, and hyaluronic acid with mineral oil as the dispersed phase to increase emulsion viscosity<sup>[105]</sup>. However, the droplet size was reported to increase overtime and the samples are required to wash in DCM to remove the oil and subsequently lyophilized at –80°C for 24 h to solidify and dry.

Extrusion-based 3D printing combined with emulsion templating can be used to create a porous ceramic that will be sintered at 1600°C for 2 h to form a solid<sup>[106]</sup>. Nanoscale porosity of 100-900 nm can be achieved using a nanodroplet-stabilized pickering emulsions which are 3D printed through direct ink writing. It shows that 3D extrusion-based printing using nanoporosity emulsions is achievable<sup>[107]</sup>. Furthermore, large 100 μm pores

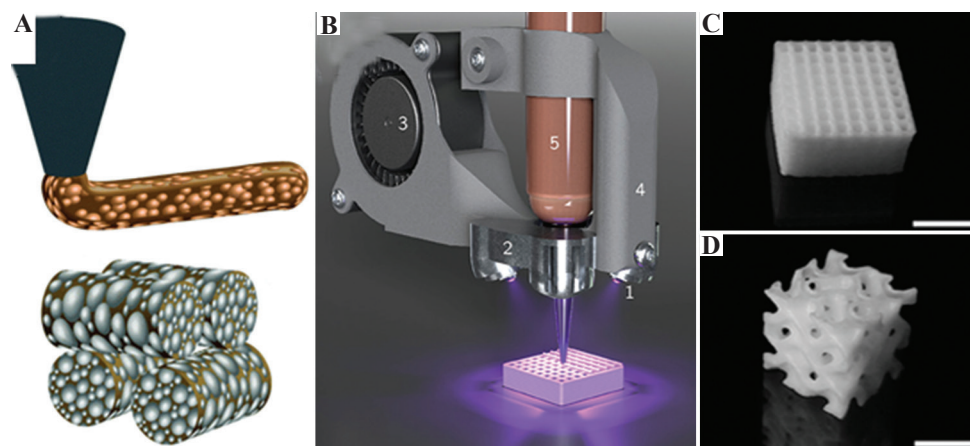


**Figure 3.** (A) 3D schematic showing an extruded silica-chitosan-based emulsion and the theoretical pore distribution within the extruded part and subsequent polymerized structure. Adapted from ref.<sup>105</sup> with permission from The Royal Society of Chemistry. (B) 3D model showing a cure-on-dispense 3D printing of a photocurable monomeric-based emulsion, (C and D) two pictures of polymerized high internal phase emulsions based structures created using this device. (B-D) Images adapted from ref.<sup>1104</sup> licensed under Creative Commons Attribution License.

were also created using sacrificial polymer beads in the emulsion, highlighting the versatility of this method to use porogens other than water for additional level of porosity control. Emulsions stabilized with submicron pickering particles can be used with a range of liquids and applied to create both micro- and nano-sized emulsion droplets<sup>[108]</sup>. SiO<sub>2</sub> nanoparticles can stabilize a styrene-based W/O emulsion which holds its shape before being thermally polymerized in an oil bath<sup>[109]</sup>. Pickering emulsions using hydrophobized silica particle can create a 140–450 nm droplet size distribution<sup>[110]</sup>. However, when particle-stabilized emulsions are used for foam templating, they typically have low interconnectivity as the particles hinder interconnecting window formation. Nevertheless, adding a small amount of surfactant fixes this by orientating itself at the contact point between adjacent droplets, creating interconnectivity windows during polymerization<sup>[111]</sup>.

Extrusion-based emulsion templating, including a variety of AM techniques, has numerous applications in tissue engineering as the inherent interconnectivity facilitates cell ingrowth<sup>[54]</sup>. These include a 3D-printed cure-on-dispense kaolin clay-loaded poly(ethylene glycol) diacrylate and methacrylate-based O/W HIPE (3 μm average porosity with 0.75 μm interconnects) with an ability to swell up to 11 times its size in buffer solution<sup>[87]</sup>. A chitosan-modified silica nanoparticle for potential drug release of 3D-printed materials has been reported, although the post-cross-linking with glutaraldehyde took up to 48 h<sup>[112]</sup>. Extrusion-based printing also lends itself useful for printing multiple materials together, such as a degradable UV curable HIPE combined with an outer thermoplastic extruded (poly(ε-caprolactone) (PCL) or poly(lactic acid) (PLA) polymer<sup>[94]</sup>.

Extrusion-based 3D printing can be applied with non-polymerizable polymers dissolved in a solvent. Here, the solvent acts as a porogen through polymer precipitation-based 3D printing. This technique uses the difference in polymer solubility between two mutually miscible solvents to inject a solvent dissolved polymer into a vat of a non-solvent to evoke rapid polymer solidification *in situ*<sup>[113]</sup>. By varying the solvent/polymer ratio within this immersion precipitation 3D printing (*ip3DP*), tunable porous structures can be created from a range of dissolvable polymers<sup>[114]</sup>. Air-based drying using a similar solvent for dissolving has been reported using a pickering polyHIPE made from degradable polymers, such as poly(l-lactic acid) (PLLA) and PCL with hydrophobically modified silica nanoparticles (h-SiO<sub>2</sub>) to both stabilize the initial emulsion and increase its viscosity. The polymers were dissolved in dichloromethane, and after printing, the solvent was evaporated to leave behind solid scaffolds, although the samples were deformed during solvent evaporation<sup>[115]</sup>. The authors reported in a follow-up study that this deformation can be avoided using hydrophobically modified hydroxyapatite (HAp) nanoparticles in the initial PCL-based pickering emulsion<sup>[116]</sup>.

There are alternative routes, other than emulsion templating, for producing porous structures. Air bubbles can be used as a porogen, either by directly printing a UV curable foamed monomer<sup>[117]</sup> or using a foam that sets by thermogelation after it has been printed<sup>[118]</sup>. Alternatively, a blowing agent can be used within the 3D-printed part, which is decomposed post-processing to expand it into a porous material<sup>[119]</sup>. Furthermore, particles such as sieved salt can be used as a sacrificial template for a monomer to cross-link around, 75 μm extra

fine salt crystals can be combined with a DLP printer and photocurable ink, although the samples had limited interconnectivity<sup>[120]</sup>. Similarly, monodisperse particles of wax or polycaprolactone can be used within a 3D-printed silk to create porosity<sup>[121]</sup>.

## 10. Emulsion reproducibility and scalability

Commercial virus filtration membranes that use size exclusion as the primary filtering mechanism require a high degree of control over the pore size distribution; where a larger pore sizes reduces the filters ability to retain the virus<sup>[122]</sup>. To create a reproducible filter using emulsion templating, every mixing aspect of the initial emulsion has to be controlled. The same mixing speed can be used; however, using mechanical mixing to break up the droplet phase creates a broad distribution of pore sizes. These include overhead stirrers (320–1260 rpm)<sup>[26]</sup> and high-speed homogenizers (25,000 rpm)<sup>[27]</sup>. A syringe pump can be used to add the droplet phase during mixing to create a more uniform droplet breakup to increase reproducibility between emulsions<sup>[28]</sup>. However, this will still produce a polydisperse droplet size distribution. Depending on the difference between the smallest and largest pores, this may be sufficient for an antiviral filter. Many large-scale emulsification techniques that are used in industries, such as the pharmaceuticals and cosmetics, could potentially be adapted<sup>[123]</sup>.

Emulsification techniques using membrane, microchannel or microfluidic-based devices can create an unprecedented level of control over emulsion droplets as well as particle synthesis<sup>[124]</sup>. A microfluidic device can create droplets one by one to produce a highly ordered monodisperse polyHIPE with precise control over pore size and interconnectivity throughout the structure<sup>[125,126]</sup> (**Figure 4**), especially when combined with the control of the locus of initiation<sup>[127]</sup>. Microfluidic-based devices can be adapted to produce bubbles of air as the dispersed phase template that produces a foamed styrene-in-water emulsion for creating a porous material<sup>[128]</sup>. In addition, when using a valve-based flow-focusing junction (vFF) within a microfluidic device, the air bubble size can be adjusted in real time to produce a porous gradient ranging from 80 to 800  $\mu\text{m}$  pores, and this method has been used to produce nanohydroxyapatite particle-loaded gelatin-based foams that were 3D printed and then sintered to produce a porous ceramic<sup>[129]</sup>. This valve-based approach can also be used for W/O emulsions<sup>[130]</sup>.

The logistics, potential benefits, and limitations regarding the upscaling of both emulsion- and foam-based templating methods to produce porous polymers have been reviewed in detail by Stubenrauch *et al.*<sup>[131]</sup>. The limitation of microfluidic setups is that droplets are made one by one. Scaled-up production of monodisperse droplets is achievable using a circularly arranged

microfluidic channels with 128 cross-junctions<sup>[132]</sup> which can be adapted to a parallelized network of channels within a coaxial annular world-to-chip interface<sup>[133]</sup>.

Membrane-based emulsification is one such way to create a scalable emulsion templating process. A monodisperse foam can potentially be continuously made using a dispersion cell, and this has recently been used for emulsion templating where the air is the dispersed phase<sup>[134]</sup>. Furthermore, other studies about membrane-based emulsions demonstrated the creation of a range of micro- and nanoemulsions with tunable droplet sizes<sup>[135]</sup> and these techniques were used to produce porous particles and materials<sup>[136]</sup>.

## 11. Challenges and future perspectives

In this review, the current research on the AM of emulsion-based inks that produce porous foams of various materials and sizes is discussed. The versatility of emulsion templating in the manufacture of porous materials and its use in 3D printing indicate that there are many potential crossovers that could adapt this technology to new applications, such as a respirator filter against bacterial and viral infections of the respiratory tract. Nevertheless, the AM aspects of this technique are still in its infancy. Therefore, precautions should be taken when choosing a specific emulsion-based AM technique. Specifically, an aerosol filter is part of the RPE that is used prevent the transmission of COVID-19.

Emulsion templating is a versatile manufacturing technique. The porosity, interconnectivity, surface chemistry, and material choice are all independent variables that can be varied depending on the desired filter requirements. A 3D-printed polyHIPE-based respirator needs to adhere to the strict classification requirements before being categorized as FFP1, FFP2, or FFP3. These requirements include being permeable to air while adhering to the required standards of air flow resistance and retaining high filter efficiency. The European standards EN 149:2001 + A1:2009 set specific criteria for this, including particle penetration determined using a NaCl aerosol generator.

PolyHIPE-based filters can be used to remove airborne particulates, such as 2.5  $\mu\text{m}$  hydrocarbon fragments from the exhaust fumes, and as a water filter which can remove 1–11  $\mu\text{m}$  suspended particulates. PolyHIPE publications relating to specific virus binding and antibacterial feature are limited but they highlight the importance of surface functionalization that leads to efficient trapping of virus-laden particles by the polymer surface. We foresee the inherent hydrophobicity of the polyHIPE created from water-in-oil emulsions being advantageous in preventing virus-containing airborne water droplets from penetrating the material. Furthermore, the tunable mechanical properties, manufacture flexibility,

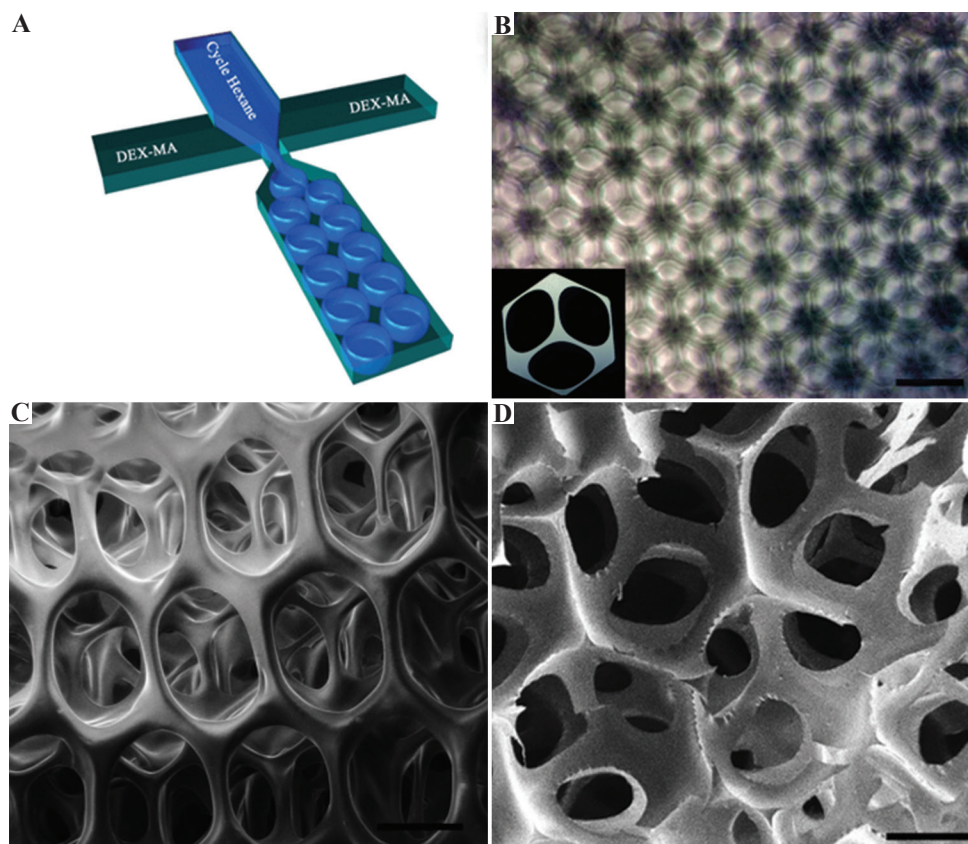


**Figure 4.** (A) A computer-generated schematic representation of the microfluidic monodisperse droplet formation. (B) Optical microscope picture of the closely packed droplets in the emulsion (scale bar 200  $\mu\text{m}$ ). (C and D) Scanning electron microscope image of the polymerized high internal phase emulsions created using this microfluidic system showing the surface and a fractured section (scale bar 100  $\mu\text{m}$ ). Images were adapted from Costantini *et al.*<sup>[125]</sup>, respectively, under the Creative Commons License.

increased temperature resistance, and potential reusability are some of its strengths.

A scalable emulsification process is required to produce reproducible emulsions with high control over porosity and interconnectivity between batches. There are many industrial emulsification tools that can meet this need. Emulsion stability needs to be considered if the printable emulsion is to be stored for an extended period. Emulsion destabilization can cause larger droplets to form at the expense of smaller ones. 3D printing of the emulsion will need to preserve the initial droplet size, not cause destabilization, and minimize the time between the creation of emulsion and its subsequent polymerization into the filter material.

From an AM perspective, an extrusion-based 3D printing is recommended as a viable printing technique for filter applications because it maintains an open outer porosity. A micro- or nanoemulsion with tightly packed water droplets has high viscosity so this type of emulsion is not suitable for stereolithography-based 3D printing as the emulsion cannot spread over the surface for layering. Furthermore, this technique has the capability to extrude multiple emulsions on the same print, giving user control over multiple materials, surface functionalities, and a

porosity gradient within the filter. All of which could be used to create a complex internal geometry that controls the air movement through the filter. Nevertheless, this is only viable for niche applications currently because 3D printing emulsion inks are a time-consuming process. Its strength lies in its customizability or complex bespoke applications that cannot be made by the traditional manufacturing techniques.

For an aerosol-based filter application that only requires a porous membrane or column, bulk polymerization is preferable over AM. Pouring the emulsion into a membrane or mold should suffice, and specific mold materials can be chosen to prevent the formation of a surface skin on the polyHIPE surface. This would also be the simplest method for producing a filter that can be brought to the market and can be incorporated into the current RPE production using 3D printing. UV or redox based cured emulsions could be the most suitable for the industrial sector because of their fast curing times.

## Acknowledgements

We would like to acknowledge funding from the Engineering and Physical Sciences Research Council (Grant no. EP/R511754/1 and EP/L505055/1).

## Conflicts of interest

No conflicts of interest were reported by all authors.

## References

- Joshi SC, Sheikh AA, 2015, 3D printing in aerospace and its long-term sustainability. *Virtual Phys Prototyping*, 10:175–85. <https://doi.org/10.1080/17452759.2015.1111519>
- Conner BP, Manogharan GP, Martof AN, *et al.*, 2014, Making Sense of 3-D Printing: Creating a Map of Additive Manufacturing Products and Services. *Addit Manuf*, 1:64–76. <https://doi.org/10.1016/j.addma.2014.08.005>
- Ng WL, Chua CK, Shen YF, 2019, Print me an organ? Why we are not there yet. *Progress Polymer Sci*, 97:101145. <https://doi.org/10.1016/j.progpolymsci.2019.101145>
- Tino R, Moore R, Antoline S, *et al.*, 2020, COVID-19 and the Role of 3D Printing in Medicine. Springer, Berlin, Germany.
- Celik HK, Kose O, Ulmeanu ME, *et al.*, 2020, Design and Additive Manufacturing of a Medical Face Shield for Healthcare Workers Battling Coronavirus (COVID-19). *Int J Bioprint*, 6:286. <https://doi.org/10.18063/ijb.v6i4.286>
- Cook TM, 2020, Personal protective equipment during the coronavirus disease (COVID) 2019 pandemic—a narrative review. *Anaesthesia*, 75:920–7. <https://doi.org/10.1111/anae.15071>
- Public Health England, 2020, COVID-19: Infection Prevention and Control Guidance. Public Health England, United Kingdom, England.
- Chen N, Zhou M, Dong X, *et al.*, 2020, Epidemiological and Clinical Characteristics of 99 Cases of 2019 Novel Coronavirus Pneumonia in Wuhan, China: A Descriptive Study. *Lancet*, 395:507–13. [https://doi.org/10.1016/s0140-6736\(20\)30211-7](https://doi.org/10.1016/s0140-6736(20)30211-7)
- World Health Organization, 2020, Rational Use of Personal Protective Equipment (PPE) for Coronavirus Disease (COVID-19): Interim Guidance. World Health Organization, Geneva, Switzerland.
- Cheng VC, Wong SC, Chuang VW, *et al.*, 2020, The Role of Community-wide Wearing of Face Mask for Control of Coronavirus Disease 2019 (COVID-19) Epidemic Due to SARS-CoV-2. *J Infect*, 81:107–14. <https://doi.org/10.1016/j.jinf.2020.04.024>
- Vuorinen V, Aarnio M, Alava M, *et al.*, 2020, Modelling Aerosol Transport and Virus Exposure with Numerical Simulations in Relation to SARS-CoV-2 Transmission by Inhalation Indoors. *Saf Sci*, 130:104866. <https://doi.org/10.1016/j.ssci.2020.104866>
- Gralton J, Tovey E, McLaws ML, *et al.*, 2011, The Role of Particle Size in Aerosolised Pathogen Transmission: A Review. *J Infect*, 62:1–13. <https://doi.org/10.1016/j.jinf.2010.11.010>
- Wang CS, Otani Y, 2013, Removal of Nanoparticles from Gas Streams by Fibrous Filters: A Review. *Ind Eng Chem Res*, 52:5–17. <https://doi.org/10.1021/ie300574m>
- Grinshpun SA, Yermakov M, Khodoun M, 2020, Autoclave Sterilization and Ethanol Treatment of Re-used Surgical Masks and N95 Respirators During COVID-19: Impact on Their Performance and Integrity. *J Hosp Infect*, 105:608–14. <https://doi.org/10.1016/j.jhin.2020.06.030>
- Rengasamy S, Eimer BC, Shaffer RE, 2009, Comparison of Nanoparticle Filtration Performance of NIOSH-approved and CE-marked Particulate Filtering Facepiece Respirators. *Ann Occup Hyg*, 53:117–28. <https://doi.org/10.1093/annhyg/men086>
- Grinshpun SA, Haruta H, Eninger RM, *et al.*, 2009, Performance of an N95 Filtering Facepiece Particulate Respirator and a Surgical Mask During Human Breathing: Two Pathways for Particle Penetration. *J Occup Environ Hyg*, 6:593–603. <https://doi.org/10.1080/15459620903120086>
- Cai M, Li H, Shen S, *et al.*, 2018, Customized Design and 3D Printing of Face Seal for an N95 Filtering Facepiece Respirator. *J Occup Environ Hyg*, 15:226–34. <https://doi.org/10.1080/15459624.2017.1411598>
- Swennen GR, Pottel L, Haers PE, 2020, Custom-made 3D-printed Face Masks in Case of Pandemic Crisis Situations with a Lack of Commercially Available FFP2/3 Masks. *Int J Oral Maxillofac Surg*, 49:673–7. <https://doi.org/10.1016/j.ijom.2020.03.015>
- British Standards Institution, 2011, 149: 2001+ A1: 2009 Respiratory Protective Devices. Filtering Half Masks to Protect against Particles. Requirements, Testing, Marking. British Standards Institution, London, UK. <https://doi.org/10.3403/02279488>
- Gawn J, Clayton M, Makison C, *et al.*, 2008, Evaluating the Protection Afforded by Surgical Masks Against Influenza Bioaerosols: Gross Protection of Surgical Masks Compared to Filtering Facepiece Respirators. *Health Safety Exec*, 2020. Available from: <https://www.hse.gov.uk/research/rrpdf/rr619.pdf>. [Last accessed on 2020 Jan 01].
- Lee SA, Hwang DC, Li HY, *et al.*, 2016, Particle Size-selective Assessment of Protection of European Standard FFP

- Respirators and Surgical Masks Against Particles-tested with Human Subjects. *J Healthc Eng*, 2016:8572493.  
<https://doi.org/10.1155/2016/8572493>
22. Langford CR, Johnson DW, Cameron NR, 2015, Preparation of Hybrid Thiol-Acrylate Emulsion-templated Porous Polymers by Interfacial Copolymerization of High Internal Phase Emulsions. *Macromol Rapid Commun*, 36:834–9.  
<https://doi.org/10.1002/marc.201400733>
  23. Carnachan RJ, Bokhari M, Przyborski SA, *et al.*, 2006, Tailoring the Morphology of Emulsion-templated Porous Polymers. *Soft Matter*, 2:608–16.  
<https://doi.org/10.1039/b603211g>
  24. Althubeiti KM, Horozov TS, 2019, Efficient Preparation of Macroporous Poly (Methyl Methacrylate) Materials from High Internal Phase Emulsion Templates. *React Function Polymers*, 142:207–12.  
<https://doi.org/10.1016/j.reactfunctpolym.2019.06.015>
  25. Moglia RS, Holm JL, Sears NA, *et al.*, 2011, Injectable polyHIPEs as High-porosity Bone Grafts. *Biomacromolecules*, 12:3621–8.  
<https://doi.org/10.1021/bm2008839>
  26. Paterson TE, Gigliobianco G, Sherborne C, *et al.*, 2018, Porous Microspheres Support Mesenchymal Progenitor Cell Ingrowth and Stimulate Angiogenesis. *APL Bioeng*, 2:026103.  
<https://doi.org/10.1063/1.5008556>
  27. Huš S, Krajnc P, 2014, PolyHIPEs from Methyl Methacrylate: Hierarchically Structured Microcellular Polymers with Exceptional Mechanical Properties. *Polymer*, 55:4420–24.  
<https://doi.org/10.1016/j.polymer.2014.07.007>
  28. Bokhari M, Carnachan RJ, Przyborski SA, *et al.*, 2007, Emulsion-templated Porous Polymers as Scaffolds for Three Dimensional Cell Culture: Effect of Synthesis Parameters on Scaffold Formation and Homogeneity. *J Mater Chem*, 17:4088–94.  
<https://doi.org/10.1039/b707499a>
  29. Richez A, Deleuze H, Vedrenne P, *et al.*, 2005, Preparation of Ultra-low-density Microcellular Materials. *J Appl Polymer Sci*, 96:2053–63.  
<https://doi.org/10.1002/app.21668>
  30. Xu H, Zheng X, Huang Y, *et al.*, 2016, Interconnected Porous Polymers with Tunable Pore Throat Size Prepared via Pickering High Internal Phase Emulsions. *Langmuir*, 32:38–45.  
<https://doi.org/10.1021/acs.langmuir.5b03037>
  31. Williams JM, Gray AJ, Wilkerson MH, 1990, Emulsion Stability and Rigid Foams from Styrene or Divinylbenzene Water-in-oil Emulsions. *Langmuir*, 6:437–44.  
<https://doi.org/10.1021/la00092a026>
  32. Cameron NR, Barbetta A, 2000, The Influence of Porogen Type on the Porosity, Surface Area and Morphology of Poly (Divinylbenzene) PolyHIPE Foams. *J Mater Chem*, 10:2466–71.  
<https://doi.org/10.1039/b003596n>
  33. Barbetta A, Cameron NR, 2004, Morphology and Surface Area of Emulsion-Derived (PolyHIPE) Solid Foams Prepared with Oil-phase Soluble Porogenic Solvents: Span 80 as Surfactant. *Macromolecules*, 37:3188–201.  
<https://doi.org/10.1021/ma0359436>
  34. Williams JM, Wroblewski DA, 1988, Spatial Distribution of the Phases in Water-in-oil Emulsions. Open and Closed Microcellular Foams from Cross-linked Polystyrene. *Langmuir*, 4:656–62.  
<https://doi.org/10.1021/la00081a027>
  35. Gurevitch I, Silverstein MS, 2010, Polymerized Pickering HIPEs: Effects of Synthesis Parameters on Porous Structure. *J Polymer Sci Part A*, 48:1516–25.  
<https://doi.org/10.1002/pola.23911>
  36. Robinson JL, Moglia RS, Stuebben MC, *et al.*, 2014, Achieving Interconnected Pore Architecture in Injectable polyHIPEs for Bone Tissue Engineering. *Tissue Eng Part A*, 20:1103–12.  
<https://doi.org/10.1089/ten.tea.2013.0319>
  37. Cameron NR, Sherrington DC, Albiston L, *et al.*, 1996, Study of the Formation of the Open-cellular Morphology of Poly (Styrene/Divinylbenzene) polyHIPE Materials by Cryo-SEM. *Coll Polymer Sci*, 274:592–5.  
<https://doi.org/10.1007/bf00655236>
  38. Lissant KJ, 1966, The Geometry of High-internal-phase-ratio Emulsions. *J Coll Int Sci*, 22:462–8.  
[https://doi.org/10.1016/0021-9797\(66\)90091-9](https://doi.org/10.1016/0021-9797(66)90091-9)
  39. Owen R, Sherborne C, Paterson T, *et al.*, 2016, Emulsion Templated Scaffolds with Tunable Mechanical Properties for Bone Tissue Engineering. *J Mech Behav Biomed Mater*, 54:159–72.  
<https://doi.org/10.1016/j.jmbbm.2015.09.019>
  40. San Manley S, Graeber N, Grof Z, *et al.*, 2009, New Insights into the Relationship Between Internal Phase Level of Emulsion Templates and Gas-liquid Permeability of Interconnected Macroporous Polymers. *Soft Matter*, 5:4780–7.  
<https://doi.org/10.1039/b900426b>
  41. Tadros TF, 2013, Emulsion Formation, Stability, and Rheology. *Emulsion Formation Stabil*, 1:1–75.  
<https://doi.org/10.1002/9783527647941.ch1>
  42. Brun N, Ungureanu S, Deleuze H, *et al.*, 2011, Hybrid Foams, Colloids and Beyond: From Design to Applications. *Chem*

- Soc Rev*, 40:771–88.  
<https://doi.org/10.1039/b920518g>
43. Cameron NR, 2005, High Internal Phase Emulsion Templating as a Route to Well-defined Porous Polymers. *Polymer*, 46:1439–49.  
<https://doi.org/10.1016/j.polymer.2004.11.097>
  44. Cameron NR, Sherrington DC, 1996, High Internal Phase Emulsions (HIPEs)-structure, Properties and Use in Polymer Preparation. *Biopolymers Liquid Crystalline Polymers Phase Emulsion*, 126:163–214.  
[https://doi.org/10.1007/3-540-60484-7\\_4](https://doi.org/10.1007/3-540-60484-7_4)
  45. Kimmins SD, Cameron NR, 2011, Functional Porous Polymers by Emulsion Templating: Recent Advances. *Adv Function Mater*, 21:211–25.  
<https://doi.org/10.1002/adfm.201001330>
  46. Pulko I, Krajnc P, 2012, High Internal Phase Emulsion Templating-a Path to Hierarchically Porous Functional Polymers. *Macromol Rapid Commun*, 33:1731–46.  
<https://doi.org/10.1002/marc.201200393>
  47. Tebboth M, Menner A, Kogelbauer A, *et al.*, 2014, Polymerised high internal phase emulsions for fluid separation applications. *Curr Opin Chem Eng*, 4:114–20.  
<https://doi.org/10.1016/j.coche.2014.03.001>
  48. Silverstein MS, 2014, PolyHIPEs: Recent Advances in Emulsion-templated Porous Polymers. *Prog Polym Sci*, 39:199–234.  
<https://doi.org/10.1016/j.progpolymsci.2013.07.003>
  49. Zhang T, Sanguramath RA, Israel S, *et al.*, 2019, Emulsion Templating: Porous Polymers and Beyond. *Macromolecules*, 52:5445–79.  
<https://doi.org/10.1021/acs.macromol.8b02576>
  50. Silverstein MS, 2014, Emulsion-templated Porous Polymers: A Retrospective Perspective. *Polymer*, 55:304–20.  
<https://doi.org/10.1016/j.polymer.2013.08.068>
  51. Silverstein MS, 2020, The Chemistry of Porous Polymers: The Holy Grail. *Israel J Chem*, 60:140–50.
  52. Andrieux S, Quell A, Stubenrauch C, *et al.*, 2018, Liquid Foam Templating-a Route to Tailor-made Polymer Foams. *Adv Coll Int Sci*, 256:276–90.  
<https://doi.org/10.1016/j.cis.2018.03.010>
  53. Moon S, Kim JQ, Kim BQ, *et al.*, 2020, Processable Composites with Extreme Material Capacities: Toward Designer High Internal Phase Emulsions and Foams. *Chem Mater*, 32:4838–54.  
<https://doi.org/10.1021/acs.chemmater.9b04952>
  54. Dikici BA, Claeysens F, 2020, Basic Principles of Emulsion Templating and Its Use as an Emerging Manufacturing Method of Tissue Engineering Scaffolds. *Front Bioeng Biotechnol*, 8:875.  
<https://doi.org/10.3389/fbioe.2020.00875>
  55. Taylor-Pashow KM, Pribyl JG, 2019, PolyHIPEs for Separations and Chemical Transformations: A Review. *Solvent Extract Ion Exchan*, 37:1–26.  
<https://doi.org/10.1080/07366299.2019.1592924>
  56. Choudhury S, Connolly D, White B, 2015, Supermacroporous polyHIPE and Cryogel Monolithic Materials as Stationary Phases in Separation Science: A Review. *Anal Methods*, 7:6967–82.  
<https://doi.org/10.1039/c5ay01193k>
  57. Gu H, Liu Y, Yin D, *et al.*, 2018, Heparin-immobilized Polymeric Monolithic Column with Submicron Skeletons and Well-defined Macropores for Highly Efficient Purification of Enterovirus 71. *Macromol Mater Eng*, 303:1800411.  
<https://doi.org/10.1002/mame.201800411>
  58. Muralikrishnan R, Swarnalakshmi M, Nakkeeran E, 2014, Nanoparticle-membrane Filtration of Vehicular Exhaust to Reduce air Pollution-a Review. *Int Res J Environ Sci*, 3:82–6.
  59. Xing YF, Xu YH, Shi MH, *et al.*, 2016, The Impact of PM2.5 on the Human Respiratory System. *J Thorac Dis*, 8:E69.
  60. ISO, 2015, ISO/TS 80004-2: 2015. Nanotechnologies-Vocabulary-Part 2: Nano-objects. ISO, United Kingdom.
  61. Ramachandran S, Rajiv S, 2020, Emulsion Templated Amine Functionalised Polymeric Monolith Filter for Innovative Air Purification Technology. *J Porous Mater*, 27:939–46.  
<https://doi.org/10.1007/s10934-019-00856-1>
  62. Walsh DC, Stenhouse JI, Kingsbury LP, *et al.*, 1996, PolyHIPE Foams: Production, Characterisation, and Performance as Aerosol Filtration Materials. *J Aerosol Sci*, 27:S629–30.  
[https://doi.org/10.1016/0021-8502\(96\)00387-4](https://doi.org/10.1016/0021-8502(96)00387-4)
  63. Hung CH, Leung WW, 2011, Filtration of Nano-aerosol Using Nanofiber Filter Under Low Peclet Number and Transitional Flow Regime. *Separat Purificat Technol*, 79:34–42.  
<https://doi.org/10.1016/j.seppur.2011.03.008>
  64. Krajnc P, Leber N, Štefanec D, *et al.*, 2005, Preparation and Characterisation of Poly (High Internal Phase Emulsion) Methacrylate Monoliths and Their Application as Separation Media. *J Chromatogr A*, 1065:69–73.  
<https://doi.org/10.1016/j.chroma.2004.10.051>
  65. Pulko I, Smrekar V, Podgornik A, *et al.*, 2011, Emulsion Templated Open Porous Membranes for Protein Purification. *J Chromatogr A*, 1218:2396–401.  
<https://doi.org/10.1016/j.chroma.2010.11.069>
  66. Yao C, Qi L, Yang G, *et al.*, 2010, Preparation of Sub-micron Skeletal Monoliths with High Capacity for Liquid



- Chromatography. *J Separat Sci*, 33:475–83.  
<https://doi.org/10.1002/jssc.200900655>
67. Dinh NP, Cam QM, Nguyen AM, *et al.*, 2009, Functionalization of Epoxy-based Monoliths for Ion Exchange Chromatography of Proteins. *J Separat Sci*, 32:2556–64.  
<https://doi.org/10.1002/jssc.200900243>
68. Zhang T, Guo Q, 2017, Continuous Preparation of polyHIPE Monoliths from Ionomer-stabilized High Internal Phase Emulsions (HIPEs) for Efficient Recovery of Spilled Oils. *Chem Eng J*, 307:812–9.  
<https://doi.org/10.1016/j.cej.2016.09.024>
69. Zhang N, Zhong S, Zhou X, *et al.*, 2016, Superhydrophobic P (St-DVB) Foam Prepared by the High Internal Phase Emulsion Technique for Oil Spill Recovery. *Chem Eng J*, 298:117–24.  
<https://doi.org/10.1016/j.cej.2016.03.151>
70. Balow RB, Giles SL, McGann CL, *et al.*, 2018, Rapid Decontamination of Chemical Warfare Agent Simulant with Thermally Activated Porous Polymer Foams. *Ind Eng Chem Res*, 57:8630–4.  
<https://doi.org/10.1021/acs.iecr.8b01546>
71. McGann CL, Daniels GC, Giles SL, *et al.*, 2018, Air Activated Self-Decontaminating Polydicyclopentadiene PolyHIPE Foams for Rapid Decontamination of Chemical Warfare Agents. *Macromol Rapid Commun*, 39:1800194.  
<https://doi.org/10.1002/marc.201800194>
72. Hughes JM, Budd PM, Tiede K, *et al.*, 2015, Polymerized High Internal Phase Emulsion Monoliths for the Chromatographic Separation of Engineered Nanoparticles. *J Appl Polymer Sci*, 132:41229.  
<https://doi.org/10.1002/app.41229>
73. Bhungara Z, 1995, Polyhipe Foam Materials as Filtration Media. *Filtrat Separat*, 32:245–51.  
[https://doi.org/10.1016/s0015-1882\(97\)84048-7](https://doi.org/10.1016/s0015-1882(97)84048-7)
74. Malakian A, Zhou M, Zowada RT, *et al.*, 2019, Synthesis and *in Situ* Functionalization of Microfiltration Membranes Via High Internal Phase Emulsion Templating. *Polymer Int*, 68:1378–86.  
<https://doi.org/10.1002/pi.5828>
75. Katsoyiannis IA, Zouboulis AI, 2002, Removal of Arsenic from Contaminated Water Sources by Sorption Onto Iron-oxide-coated Polymeric Materials. *Water Res*, 36:5141–55.  
[https://doi.org/10.1016/s0043-1354\(02\)00236-1](https://doi.org/10.1016/s0043-1354(02)00236-1)
76. Zhu Y, Wang W, Yu H, *et al.*, 2020, Preparation of Porous Adsorbent Via Pickering Emulsion Template for Water Treatment: A Review. *J Environ Sci*, 88:217–36.  
<https://doi.org/10.1016/j.jes.2019.09.001>
77. Zhao C, Danish E, Cameron NR, *et al.*, 2007, Emulsion-templated Porous Materials (PolyHIPEs) for Selective Ion and Molecular Recognition and Transport: Applications in Electrochemical Sensing. *J Mater Chem*, 17:2446–53.  
<https://doi.org/10.1039/b700929a>
78. Pulko I, Krajnc P, 2008, Open Cellular Reactive Porous Membranes from High Internal Phase Emulsions. *Chem Commun*, 37:4481–3.  
<https://doi.org/10.1039/b807095d>
79. Sevšek U, Seifried S, Stropnik Č, *et al.*, 2011, Poly (styrene-co-divinylbenzene-co-2-ethylhexyl) Acrylate Membranes with Interconnected Macroporous Structure. *Mater Tehnol*, 45:247–51.
80. Kovačič S, Preishuber-Pflügl F, Slugovc C, 2014, Macroporous Polyolefin Membranes from Dicyclopentadiene High Internal Phase Emulsions: Preparation and Morphology Tuning. *Macromol Mater Eng*, 299:843–50.  
<https://doi.org/10.1002/mame.201300400>
81. Owen R, Sherborne C, Evans R, *et al.*, 2020, Combined Porogen Leaching and Emulsion Templating to Produce Bone Tissue Engineering Scaffolds. *Int J Bioprint*, 6:99–113.  
<https://doi.org/10.18063/ijb.v6i2.265>
82. Huang X, Yang Y, Shi J, *et al.*, 2015, High-internal-phase Emulsion Tailoring Polymer Amphiphilicity towards an Efficient NIR-sensitive Bacteria Filter. *Small*, 11:4876–83.  
<https://doi.org/10.1002/smll.201501396>
83. Yang Q, Li H, Shen S, *et al.*, 2018, Study of the Micro-climate and Bacterial Distribution in the Dead-space of N95 Filtering Face Respirators. *Sci Rep*, 8:1–13.  
<https://doi.org/10.1038/s41598-018-35693-w>
84. Wang X, Chen X, Peng Y, *et al.*, 2019, Silver-modified Porous Polystyrene Sulfonate Derived from Pickering High Internal Phase Emulsions for Capturing Lithium-ion. *RSC Adv*, 9:7228–37.  
<https://doi.org/10.1039/c8ra09740b>
85. Sadeghi S, Moghbeli MR, 2012, Synthesis and Dispersion of Colloidal Silver Nanoparticles on Microcellular Polyhipe Support. *Coll Surf A*, 409:42–51.  
<https://doi.org/10.1016/j.colsurfa.2012.05.037>
86. Lundin JG, McGann CL, Weise NK, *et al.*, 2019, Iodine Binding and Release from Antimicrobial Hemostatic Polymer Foams. *React Function Polymers*, 135:44–51.  
<https://doi.org/10.1016/j.reactfunctpolym.2018.12.009>
87. Streifel BC, Lundin JG, Sanders AM, *et al.*, 2018, Hemostatic and Absorbent PolyHIPE-Kaolin Composites for 3D Printable Wound Dressing Materials. *Macromol Biosci*, 18:1700414.  
<https://doi.org/10.1002/mabi.201700414>

88. McDonnell G, Russell AD, 1999, Antiseptics and Disinfectants: Activity, Action, and Resistance. *Clin Microbiol Rev*, 12:147–79.  
<https://doi.org/10.1128/cmr.12.1.147>
89. McGann CL, Streifel BC, Lundin JG, *et al.*, 2017, Multifunctional polyHIPE Wound Dressings for the Treatment of Severe Limb Trauma. *Polymer*, 126:408–18.  
<https://doi.org/10.1016/j.polymer.2017.05.067>
90. Dikici BA, Dikici S, Reilly GC, *et al.*, 2019, A Novel Bilayer Polycaprolactone Membrane for Guided Bone Regeneration: Combining Electrospinning and Emulsion Templating. *Materials*, 12:2643.  
<https://doi.org/10.3390/ma12162643>
91. Gui H, Zhang T, Ji S, *et al.*, 2020, Nanofibrous, Porous Monoliths Formed from Gelating High Internal Phase Emulsions Using Syndiotactic Polystyrene. *Polymer*, 2020:122708.  
<https://doi.org/10.1016/j.polymer.2020.122708>
92. Johnson DW, Sherborne C, Didsbury MP, *et al.*, 2013, Macrostructuring of Emulsion-templated Porous Polymers by 3D Laser Patterning. *Adv Mater*, 25:3178–81.  
<https://doi.org/10.1002/adma.201300552>
93. Sears NA, Dhavalikar PS, Cosgriff-Hernandez EM, 2016, Emulsion Inks for 3D Printing of High Porosity Materials. *Macromol Rapid Commun*, 37:1369–74.  
<https://doi.org/10.1002/marc.201600236>
94. Sears N, Dhavalikar P, Whitely M, *et al.*, 2017, Fabrication of Biomimetic Bone Grafts with Multi-material 3D Printing. *Biofabrication*, 9:025020.  
<https://doi.org/10.1088/1758-5090/aa7077>
95. Welch CF, Rose GD, Malotky D, *et al.*, 2006, Rheology of High Internal Phase Emulsions. *Langmuir*, 22:1544–50.  
<https://doi.org/10.1021/la052207h>
96. Stansbury JW, Idacavage MJ, 2016, 3D Printing with Polymers: Challenges Among Expanding Options and Opportunities. *Dent Mater*, 32:54–64.  
<https://doi.org/10.1016/j.dental.2015.09.018>
97. Malayeri A, Sherborne C, Paterson T, *et al.*, 2016, Osteosarcoma Growth on Trabecular Bone Mimicking Structures Manufactured Via Laser Direct Write. *Int J Bioprint*, 2:67–77.  
<https://doi.org/10.18063/ijb.2016.02.005>
98. Wang AJ, Paterson T, Owen R, *et al.*, 2016, Photocurable High Internal Phase Emulsions (HIPEs) Containing Hydroxyapatite for Additive Manufacture of Tissue Engineering Scaffolds with Multi-scale Porosity. *Mater Sci Eng C*, 67:51–8.  
<https://doi.org/10.1016/j.msec.2016.04.087>
99. Sherborne C, Owen R, Reilly GC, *et al.*, 2018, Light-based Additive Manufacturing of PolyHIPEs: Controlling the Surface Porosity for 3D Cell Culture Applications. *Mater Design*, 156:494–503.  
<https://doi.org/10.1016/j.matdes.2018.06.061>
100. Huan S, Mattos BD, Ajdary R, *et al.*, 2019, Two-phase Emulgels for Direct Ink Writing of Skin-Bearing Architectures. *Adv Function Mater*, 29:1902990.  
<https://doi.org/10.1002/adfm.201902990>
101. Sušec M, Ligon SC, Stampfl J, *et al.*, 2013, Hierarchically Porous Materials from Layer-by-layer Photopolymerization of High Internal Phase Emulsions. *Macromol Rapid Commun*, 34:938–43.  
<https://doi.org/10.1002/marc.201300016>
102. Rezanavaz R, 2018, 3D Printing of Porous Polymeric Materials for Stationary Phases of Chromatography Columns. UC Library, California.
103. Cooperstein I, Layani M, Magdassi S, 2015, 3D Printing of Porous Structures by UV-Curable O/W Emulsion for Fabrication of Conductive Objects. *J Mater Chem C*, 3:2040–4.  
<https://doi.org/10.1039/c4tc02215g>
104. Wenger L, Radtke CP, Göpper J, *et al.*, 2020, 3D-printable and Enzymatically Active Composite Materials Based on Hydrogel-filled High Internal Phase Emulsions. *Front Bioeng Biotechnol*, 8:713.  
<https://doi.org/10.3389/fbioe.2020.00713>
105. Sears NA, Wilems TS, Gold KA, *et al.*, 2019, Hydrocolloid Inks for 3D Printing of Porous Hydrogels. *Adv Mater Technol*, 4:1800343.  
<https://doi.org/10.1002/admt.201800343>
106. Minas C, Carnelli D, Tervoort E, *et al.*, 2016, 3D Printing of Emulsions and Foams into Hierarchical Porous Ceramics. *Adv Mater*, 28:9993–9.  
<https://doi.org/10.1002/adma.201603390>
107. Alison L, Menasce S, Bouville F, *et al.*, 2019, 3D Printing of Sacrificial Templates into Hierarchical Porous Materials. *Sci Rep*, 9:1–9.  
<https://doi.org/10.1038/s41598-018-36789-z>
108. Jiang H, Sheng Y, Ngai T, 2020, Pickering Emulsions: Versatility of Colloidal Particles and Recent Applications. *Curr Opin Coll Int Sci*, 49:1–15.  
<https://doi.org/10.1016/j.cocis.2020.04.010>
109. Liu J, Wang P, He Y, *et al.*, 2019, Polymerizable Nonconventional Gel Emulsions and Their Utilization in the Template Preparation of Low-density, High-strength Polymeric Monoliths and 3D Printing. *Macromolecules*, 52:2456–63.

- <https://doi.org/10.1021/acs.macromol.8b02610>
110. Sihler S, Schrade A, Cao Z, *et al.*, 2015, Inverse Pickering Emulsions with Droplet Sizes Below 500 nm. *Langmuir*, 31:10392–401.  
<https://doi.org/10.1021/acs.langmuir.5b02735>
  111. Zhu W, Zhu Y, Zhou C, *et al.*, 2019, Pickering Emulsion-templated Polymers: Insights into the Relationship Between Surfactant and Interconnecting Pores. *RSC Adv*, 9:18909–16.  
<https://doi.org/10.1039/c9ra03186c>
  112. Sommer MR, Alison L, Minas C, *et al.*, 2017, 3D Printing of Concentrated Emulsions into Multiphase Biocompatible Soft Materials. *Soft Matter*, 13:1794–803.  
<https://doi.org/10.1039/c6sm02682f>
  113. Tu R, Sprague E, Sodano HA, 2020, Precipitation Printing Towards Diverse Materials, Mechanical Tailoring and Functional Devices. *Addit Manuf*, 2020:101358.  
<https://doi.org/10.1016/j.addma.2020.101358>
  114. Karyappa R, Ohno A, Hashimoto M, 2019, Immersion Precipitation 3D Printing (ip 3DP). *Mater Horiz*, 6:1834–44.  
<https://doi.org/10.1039/c9mh00730j>
  115. Yang T, Hu Y, Wang C, *et al.*, 2017, Fabrication of Hierarchical Macroporous Biocompatible Scaffolds by Combining Pickering High Internal Phase Emulsion Templates with Three-dimensional Printing. *ACS Appl Mater Int*, 9:22950–8.  
<https://doi.org/10.1021/acsami.7b05012.s001>
  116. Hu Y, Wang J, Li X, *et al.*, 2019, Facile Preparation of Bioactive Nanoparticle/Poly ( $\epsilon$ -caprolactone) Hierarchical Porous Scaffolds Via 3D Printing of High Internal Phase Pickering Emulsions. *J Coll Int Sci*, 545:104–15.  
<https://doi.org/10.1016/j.jcis.2019.03.024>
  117. Visser CW, Amato DN, Mueller J, *et al.*, 2019, Architected Polymer Foams via Direct Bubble Writing. *Adv. Mater*, 31:1904668.  
<https://doi.org/10.1002/adma.201904668>
  118. Voisin HP, Gordeyeva K, Siqueira G, *et al.*, 2018, 3D Printing of Strong Lightweight Cellular Structures Using Polysaccharide-based Composite Foams. *ACS Sustain Chem Eng*, 6:17160–7.  
<https://doi.org/10.1021/acssuschemeng.8b04549>
  119. Wirth DM, Jaquez A, Gandarilla S, *et al.*, 2020, Highly Expandable Foam for Lithographic 3D Printing. *ACS Appl Mater Int*, 12:19033–43.  
<https://doi.org/10.1021/acsami.0c02683>
  120. Mu X, Bertron T, Dunn C, *et al.*, 2017, Porous Polymeric Materials by 3D Printing of Photocurable Resin. *Mater Horiz*, 4:442–9.  
<https://doi.org/10.1039/c7mh00084g>
  121. Sommer MR, Schaffner M, Carnelli D, *et al.*, 2016, 3D Printing of Hierarchical Silk Fibroin Structures. *ACS Appl Mater Int*, 8:34677–85.  
<https://doi.org/10.1021/acsami.6b11440>
  122. Giglia S, Bohonak D, Greenhalgh P, *et al.*, 2015, Measurement of Pore Size Distribution and Prediction of Membrane Filter Virus Retention Using Liquid-liquid Porometry. *J Memb Sci*, 476:399–409.  
<https://doi.org/10.1016/j.memsci.2014.11.053>
  123. Schultz S, Wagner G, Urban K, *et al.*, 2004, High-pressure Homogenization as a Process for Emulsion Formation. *Chem Eng Technol*, 27:361–8.  
<https://doi.org/10.1002/ceat.200406111>
  124. Vladislavljević GT, 2016, Recent Advances in the Production of Controllable Multiple Emulsions Using Microfabricated Devices. *Particuology*, 24:1–17.  
<https://doi.org/10.1016/j.partic.2015.10.001>
  125. Costantini M, Colosi C, Guzowski J, *et al.*, 2014, Highly Ordered and Tunable Polyhypes by Using Microfluidics. *J Mater Chem B*, 2:2290–300.  
<https://doi.org/10.1039/c3tb21227k>
  126. Quell A, Elsing J, Drenckhan W, *et al.*, 2015, Monodisperse Polystyrene Foams Via Microfluidics—a Novel Templating Route. *Adv Eng Mater*, 17:604–9.  
<https://doi.org/10.1002/adem.201500040>
  127. Quell A, de Bergolis B, Drenckhan W, *et al.*, 2016, How the Locus of Initiation Influences the Morphology and the Pore Connectivity of a Monodisperse Polymer Foam. *Macromolecules*, 49:5059–67.  
<https://doi.org/10.1021/acs.macromol.6b00494>
  128. Elsing J, Stefanov T, Gilchrist MD, *et al.*, 2017, Monodisperse Polystyrene Foams Via Polymerization of Foamed Emulsions: Structure and Mechanical Properties. *Phys Chem Chem Phys*, 19:5477–5485.  
<https://doi.org/10.1039/c6cp06612g>
  129. Costantini M, Jaroszewicz J, Kozioł Ł, *et al.*, 2019, 3D-printing of Functionally Graded Porous Materials Using On-demand Reconfigurable Microfluidics. *Ange Chem Int Ed*, 58:7620–7625.  
<https://doi.org/10.1002/anie.201900530>
  130. Abate AR, Romanowsky MB, Agresti JJ, *et al.*, 2009, Valve-based Flow Focusing for Drop Formation. *Appl Phys Lett*, 94:023503.  
<https://doi.org/10.1063/1.3067862>
  131. Stubenrauch C, Menner A, Bismarck A, *et al.*, 2018, Emulsion and Foam Templating-promising Routes to Tailor-made Porous Polymers. *Ange Chem Int Ed*, 57:10024–10032.  
<https://doi.org/10.1002/anie.201801466>

132. Nisisako T, Torii T, 2008, Microfluidic Large-scale Integration on a Chip for Mass Production of Monodisperse Droplets and Particles. *Lab Chip*, 8:287–293.  
<https://doi.org/10.1039/b713141k>
133. Nisisako T, Ando T, Hatsuzawa T, 2012, High-volume Production of Single and Compound Emulsions in a Microfluidic Parallelization Arrangement Coupled with Coaxial Annular World-to-chip Interfaces. *Lab Chip*, 12:3426–3435.  
<https://doi.org/10.1039/c2lc40245a>
134. Carballido L, Dabrowski ML, Dehli F, *et al.*, 2020, Monodisperse Liquid Foams Via Membrane Foaming. *J Coll Int Sci*, 568:46–53.  
<https://doi.org/10.1016/j.jcis.2020.02.036>
135. Vladislavljević GT, 2019, Preparation of Microemulsions and Nanoemulsions by Membrane Emulsification. *Coll Surf A*, 2019:123709.  
<https://doi.org/10.1016/j.colsurfa.2019.123709>
136. Wang B, Prinsen P, Wang H, *et al.*, 2017, Macroporous Materials: Microfluidic Fabrication, Functionalization and Applications. *Chem Soc Rev*, 46:855–914.  
<https://doi.org/10.1039/c5cs00065c>